Dynamics and Control of Three-Dimensional Slosh in a Moving Rectangular Liquid Container Undergoing Planar Excitations

Qiang Zang and Jie Huang

***Abstract*—While significant work has been directed at suppressing the 2-D slosh, less success has been achieved with reducing the 3-D slosh in a moving rectangular container. Control of the 3-D slosh in a moving rectangular liquid container is very challenging because there are two fundamental modes and an infinite number of high modes. The dynamics of the 3-D slosh in a moving rectangular container are derived. The theoretic analysis shows that both the two fundamental and high modes have large impacts on the sloshing dynamics. A command smoothing technique is designed to suppress slosh for the two fundamental and high modes. Comparing with the combined input shaper and the low-pass filter scheme, the presented smoother provides more robustness to variations in the sloshing frequency. Simulations over a large range of various working conditions and system parameters are conducted to analyze the liquid sloshing dynamics and the robustness of the method. Experimental results obtained from a moving rectangular liquid container validate the simulated sloshing dynamics behavior and the effectiveness of the method.**

***Index Terms*—Fluid dynamics, rectangular container, robustness, 3-D slosh, vibration control.**

I. Introduction

SLOSH in a partially filled container is very common in many engineering applications [1]. The system dynamics and response can be significantly influenced by the slosh. The interaction of the slosh with the container might lead to instabilities in some cases [2]–[4]. Thus, it is critical to design a controller that can effectively suppress slosh to maintain safe operations.

Numerous researchers have worked to provide solutions to the challenging problems posed by the sloshing dynamics. Some techniques are passive to dissipate slosh energy by using absorbers or baffles [5]–[7]. However, the passive techniques add unnecessary weight and complexity to the overall system. A further solution addressed to slosh suppression is the implementation of the active control [8]. Some schemes use the container motion as the control input in a feedback control loop, such as proportional–integral–derivative control [9], sliding-mode control [10]–[13], H_∞ control [14], [15], and Lyapunov-based feedback control [16]–[18]. Some control techniques filter the input to create a prescribed motion that results in minimal slosh, such as infinite impulse response filter [19], acceleration compensation [20], and input shaping [21]–[24]. In addition, there are significant works on the modeling of slosh [25]–[27] and the construction of experimental test rigs [28], [29].

However, much of the work has concentrated on the 2-D slosh. Some efforts have focused on reducing residual vibrations for the 3-D slosh. Yano and Terashima [30] and Yano *et al.* [31], presented a hybrid-shaped approach to suppress residual slosh when a cylindrical container was transferred in a 3-D path. Experimental results demonstrated the effectiveness of the method on a moving cylindrical container. However, few papers have investigated eliminating the 3-D slosh in a moving rectangular container. The control of the 3-D sloshing dynamics in a moving rectangular container is very challenging because there are two fundamental modes and an infinite number of high modes. The two fundamental modes both have large effects on the sloshing dynamics. In addition, the high modes might have some impacts on the sloshing dynamics. Therefore, the study is essential for suppressing both the two fundamental modes and an infinite number of high modes for the 3-D slosh in a moving rectangular container. The contribution of this paper is a command smoothing technique to suppress the 3-D slosh in a moving rectangular liquid container. This paper also shows simulated and experimental verification of the method that is robust to parameter variations. Furthermore, the presented method will also benefit control of many types of underactuated systems [32]–[34].

The remainder of this paper is organized as follows. In Section II, the 3-D sloshing dynamics in a moving rectangular container is modeled. A control scheme for suppressing the overall sloshing modes is proposed in Section III. Simulations over a wide range of conditions are performed to validate the effectiveness and robustness of the method. Finally, experiments on a moving rectangular container are performed to verify the dynamic behavior of slosh and the robustness of the control scheme in Section IV.

II. Sloshing Dynamics

Fig. 1 shows a schematic representation of the 3-D slosh in a moving rectangular liquid container. A rectangular tank of length a and width b contains a fluid whose surface at rest is at height, h, from the bottom of the tank. η denotes the fluid surface elevation measured from the undisturbed free surface.

Manuscript received March 31, 2014; revised July 12, 2014; accepted September 6, 2014. Date of publication October 8, 2014; date of current version March 6, 2015.

The authors are with the School of Mechanical Engineering, Beijing Institute of Technology, Beijing 100081, China (e-mail: 971829109@qq.com; bit_huangjie@bit.edu.cn).

Color versions of one or more of the figures in this paper are available online at http://ieeexplore.ieee.org.

Digital Object Identifier 10.1109/TIE.2014.2361799

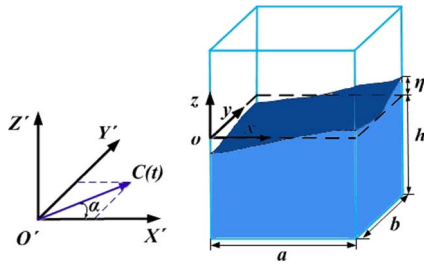

Fig. 1. Three-dimensional slosh model in a moving rectangular container.

Motion of the container is divided into the linear movement of the container along the directions, X' and Y', in the inertial Newtonian frame. These parameters are defined as functions of the input variables: the acceleration, $C(t)$, of the container and steering angle, α, between the acceleration and the X' direction. Let $oxyz$ be the moving coordinates fixed to the tank such that the oxy plane coincides with the undisturbed free surface. Note that axes of the moving coordinate system are parallel to the inertial Newtonian frame.

The fluid in the container is assumed to be incompressible and inviscid. It is also assumed that the flow is irrotational, and the displacement and velocity of the liquid free surface are small. The container is also assumed to be rigid and impermeable. For irrotational flow motions, the absolute velocity of the fluid in the container can be written as

$$v = v_0 + \nabla\varphi \tag{1}$$

where v_0 is the velocity of the tank, ∇ is the gradient operator, and φ is the perturbed velocity potential function [35]. By employing the aforementioned assumptions, the complete formulation of the boundary value problem in terms of the perturbed velocity potential in the moving coordinate system is summarized as follows [35]:

$$\nabla^2\varphi = 0 \tag{2}$$

$$\frac{\partial\varphi}{\partial x}\Big|_{x=0,a} = 0 \tag{3}$$

$$\frac{\partial\varphi}{\partial y}\Big|_{y=0,b} = 0 \tag{4}$$

$$\frac{\partial\varphi}{\partial z}\Big|_{z=-h} = 0 \tag{5}$$

$$\frac{\partial\varphi}{\partial z} = \frac{\partial\eta}{\partial t} \quad \text{at } z=\eta(x,y,t) \tag{6}$$

$$\frac{\partial\varphi}{\partial t} + g\eta + xC(t)\cos\alpha + yC(t)\sin\alpha = 0 \text{ at } z=\eta(x,y,t) \tag{7}$$

where g is the gravitational constant. The perturbed velocity potential function, φ, and surface elevation, η, can be written in the form

$$\varphi(x,y,z,t) = \sum_{ij}\phi_{ij}(x,y,z)\dot{q}_{ij}(t) \tag{8}$$

$$\eta(x,y,z,t) = \sum_{ij}H_{ij}(x,y,z)q_{ij}(t) \tag{9}$$

where i and j are nonnegative integers, $q_{ij}(t)$ is the time-dependent function, and $\phi_{ij}(x,y,z)$ and $H_{ij}(x,y,z)$ are the corresponding spatial functions. They are the solutions of the following equations:

$$\nabla^2\phi_{ij} = 0 \tag{10}$$

$$\frac{\partial\phi_{ij}}{\partial x}\Big|_{x=0,a} = 0 \tag{11}$$

$$\frac{\partial\phi_{ij}}{\partial y}\Big|_{y=0,b} = 0 \tag{12}$$

$$\frac{\partial\phi_{ij}}{\partial z}\Big|_{z=-h} = 0 \tag{13}$$

$$\frac{\partial\phi_{ij}}{\partial z} = H_{ij} = \frac{\omega_{ij}^2\phi_{ij}}{g} \text{ at } z=\eta(x,y,t). \tag{14}$$

Solving (10)–(14), we get the natural frequencies, ω_{ij}, of the sloshing modes, and the functions, ϕ_{ij} and H_{ij} [36]

$$\omega_{ij}^2 = g\pi\sqrt{\left(\frac{i}{a}\right)^2+\left(\frac{j}{b}\right)^2}\cdot\tanh\left[\pi h\sqrt{\left(\frac{i}{a}\right)^2+\left(\frac{j}{b}\right)^2}\right] \tag{15}$$

$$\phi_{ij} = \cos\left(\frac{i\pi x}{a}\right)\cos\left(\frac{j\pi y}{b}\right)\cdot\cosh\left[\pi(z+h)\sqrt{\left(\frac{i}{a}\right)^2+\left(\frac{j}{b}\right)^2}\right] \tag{16}$$

$$H_{ij} = \frac{\omega_{ij}^2\phi_{ij}}{g}. \tag{17}$$

The natural frequencies of the sloshing modes are functions of the container size and liquid depth. Note that ω_{i0} and ω_{0j} are frequencies for the transverse modes and the longitudinal modes, respectively. The set $\{\omega_{ij}, i\neq 0\ \&\ j\neq 0\}$ represents frequencies of the mixed modes. Substituting (8) and (9) into (7), then multiplying by ϕ_{ij} and integrating over the free surface $(0\le x\le a; 0\le y\le b)$ yields [37]

$$\lambda_{ij}\ddot{q}_{ij}(t) + \lambda_{ij}\omega_{ij}^2 q_{ij}(t) + \gamma_{ij}C(t)\cos\alpha + \beta_{ij}C(t)\sin\alpha = 0 \tag{18}$$

where

$$\lambda_{ij} = \rho\int_0^a\int_0^b H_{ij}\phi_{ij}\,dx\,dy \tag{19}$$

$$\gamma_{ij} = \rho\int_0^a\int_0^b xH_{ij}\,dx\,dy \tag{20}$$

$$\beta_{ij} = \rho\int_0^a\int_0^b yH_{ij}\,dx\,dy. \tag{21}$$

ρ is the density of the liquid. From (20) and (21), γ_{ij} and β_{ij} are given by

$$\gamma_{ij} = \begin{cases} \frac{-2a^2\rho\omega_{ij}^2\cosh\left(\frac{i\pi h}{a}\right)}{g\pi^2 i^2}, & i=\text{odd}, j=0 \\ 0, & \text{others} \end{cases} \tag{22}$$

$$\beta_{ij} = \begin{cases} \frac{-2b^2\rho\omega_{ij}^2\cosh\left(\frac{j\pi h}{b}\right)}{g\pi^2 j^2}, & i=0, j=\text{odd} \\ 0, & \text{others.} \end{cases} \tag{23}$$

It indicates that the acceleration in the y-direction cannot excite the transverse modal response, and the longitudinal modal response will not be excited by the acceleration in the x-direction. Meanwhile, the mixed modal response cannot be excited. From (22) and (23) and with the inclusion of the proportional damping, (18) could be changed

$$\ddot{q}_{i0}(t)+2\zeta_{i0}\omega_{i0}\dot{q}_{i0}(t)+\omega_{i0}^2 q_{i0}(t)+\frac{\gamma_{i0}}{\lambda_{i0}}C(t)\cos\alpha=0,\ i=\text{odd} \tag{24}$$

$$\ddot{q}_{0j}(t)+2\zeta_{0j}\omega_{0j}\dot{q}_{0j}(t)+\omega_{0j}^2 q_{0j}(t)+\frac{\beta_{0j}}{\lambda_{0j}}C(t)\sin\alpha=0,\ j=\text{odd} \tag{25}$$

where ζ_{i0} and ζ_{0j} are the damping ratios of the transverse and longitudinal modes, respectively. Theoretical analysis for the damping ratio has been developed to be approximately 0.01 for water [22], [38], [39]. Substituting (17) into (9) yields the surface elevation at the measurement point

$$\begin{aligned}\eta(x,y,0,t) &= \sum_{i=\text{odd},j=0} H_{ij}(x,y,0)q_{ij}(t) \\ &\quad + \sum_{i=0,j=\text{odd}} H_{ij}(x,y,0)q_{ij}(t) \\ &= \sum_{i=\text{odd}} \frac{\omega_{i0}^2\phi_{i0}}{g}q_{i0}(t) + \sum_{j=\text{odd}} \frac{\omega_{0j}^2\phi_{0j}}{g}q_{0j}(t).\end{aligned} \tag{26}$$

From (24)–(26), the transfer function of the surface elevation at the diagonal corner of the container is given by

$$\begin{aligned}\eta_{x=a,y=b,z=0}(s) &= \sum_{i=\text{odd}} \frac{-4a\omega_{i0}^2\cdot C(s)\cos\alpha}{g\pi^2 i^2\left(s^2+2\zeta_{i0}\omega_{i0}s+\omega_{i0}^2\right)} \\ &\quad + \sum_{j=\text{odd}} \frac{-4b\omega_{0j}^2\cdot C(s)\sin\alpha}{g\pi^2 j^2\left(s^2+2\zeta_{0j}\omega_{0j}s+\omega_{0j}^2\right)}.\end{aligned} \tag{27}$$

In addition, substituting (22), (23), (16) into (8) yields the transfer function of the perturbed velocity potential function at the diagonal corner of the container

$$\begin{aligned}\varphi_{x=a,y=b,z=0}(s) &= \sum_{i=\text{odd}} \frac{-4as\cdot C(s)\cos\alpha}{\pi^2 i^2\left(s^2+2\zeta_{i0}\omega_{i0}s+\omega_{i0}^2\right)} \\ &\quad + \sum_{j=\text{odd}} \frac{-4bs\cdot C(s)\sin\alpha}{\pi^2 j^2\left(s^2+2\zeta_{0j}\omega_{0j}s+\omega_{0j}^2\right)}.\end{aligned} \tag{28}$$

Thus, the theoretical analysis indicates that both the surface elevation and the perturbed velocity potential are the sum of the responses for each of an infinite number of sloshing modes along the two directions, and the slosh resulting from the accelerations along the two directions are independent.

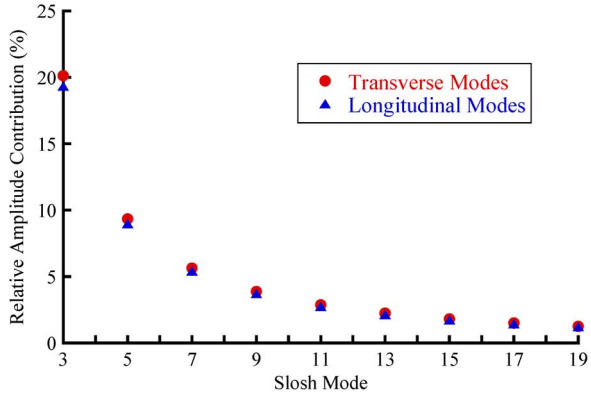

Fig. 2. Relative amplitude contributions of the transverse and longitudinal modes.

TABLE I
NOMINAL PARAMETERS

Parameter	
Container length a	182 mm
Container width b	102 mm
Maximum velocity	0.2 m/s
Driving acceleration $C(t)$	2 m/s^2
Damping ratio ζ_{ij}	0.01

From (27), the amplitude of surface elevation response from an impulse command at time zero is

$$A_{x=a,y=b,z=0}=\sum_{i=\text{odd}}\frac{-4a\omega_{i0}\cos\alpha}{g\pi^2 i^2\sqrt{1-\zeta_{i0}^2}}+\sum_{j=\text{odd}}\frac{-4b\omega_{0j}\sin\alpha}{g\pi^2 j^2\sqrt{1-\zeta_{0j}^2}}. \tag{29}$$

To better identify the amplitude contribution of each sloshing mode to the whole system, the ratio of the vibration amplitude of the impulse response from the high mode to that from the first mode is used. This ratio is called relative amplitude contribution, c. Then, (29) can be changed

$$A_{x=a,y=b,z=0}=\frac{-4a\omega_{10}\cos\alpha}{g\pi^2\sqrt{1-\zeta_{10}^2}}\cdot\sum_{i=\text{odd}}c_{i0}+\frac{-4b\omega_{01}\sin\alpha}{g\pi^2\sqrt{1-\zeta_{01}^2}}\cdot\sum_{j=\text{odd}}c_{0j} \tag{30}$$

where ω_{10} and ζ_{10} are the frequency and damping ratio for the first mode along the transverse direction, ω_{01} and ζ_{01} are those along the longitudinal direction, and the variables c_{i0} and c_{0j} are given by

$$c_{i0}=\frac{\omega_{i0}\sqrt{1-\zeta_{10}^2}}{i^2\omega_{10}\sqrt{1-\zeta_{i0}^2}},\quad i=\text{odd} \tag{31}$$

$$c_{0j}=\frac{\omega_{0j}\sqrt{1-\zeta_{01}^2}}{j^2\omega_{01}\sqrt{1-\zeta_{0j}^2}},\quad j=\text{odd}. \tag{32}$$

Thus, the amplitude of surface elevation response is produced by multiplying the sum of the relative amplitude contributions by the vibration amplitude from the first mode.

Fig. 2 illustrates the relative amplitude contribution of each sloshing mode with a liquid depth of 90 mm. The testing parameters used in this paper are given in Table I. The relative amplitude contribution of the third, the fifth, and the seventh

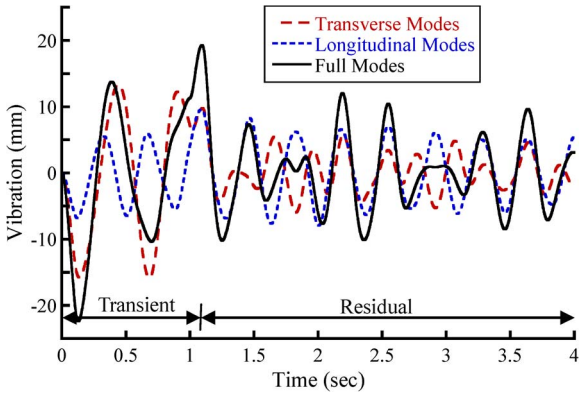

Fig. 3. Slosh response resulting from the two directions.

transverse mode are 20.1%, 9.4%, and 5.6%, respectively. Meanwhile, the relative amplitude contribution of the third, the fifth, and the seventh longitudinal mode are 19.3%, 9.0%, and 5.4%, respectively. The relative amplitude contribution decreases with increasing slosh mode. However, the sum of the relative amplitude contributions from the ninth transverse mode to the nineteenth transverse mode is 13.5%, and that from the ninth longitudinal mode to the 19th longitudinal mode is 13.0%. It shows that high sloshing modes have some impacts on the whole system. Thus, it is essential for a control scheme to suppress slosh induced by total modes.

The original command used to drive the container is a trapezoidal-velocity profile. There are two stages in the system response. The transient stage is defined as the time frame when the container is in motion. The peak-to-peak deflection during the transient stage is referred to as the transient deflection. The residual stage is defined as the time frame when the container is stopped. The peak-to-peak deflection during the residual stage is defined as the residual amplitude.

Fig. 3 shows the simulated responses from the first ten modes along the two directions when the resultant driving distance, driving angle, and liquid depth were fixed at 20 cm, 30°, and 90 mm, respectively. The transient deflection of the transverse modes, longitudinal modes, and full modes are 29.1, 16.3, and 41.6 mm, respectively. Meanwhile, the residual amplitude of the transverse modes, longitudinal modes, and full modes are 15.7, 17.3, and 29.4 mm, respectively. Simulated results indicate that the whole system response is the sum of the responses along each of the two directions. Both the two fundamental modes have significant effects on the sloshing dynamics. Thus, there is a need for a controller that can effectively suppress slosh induced by both the two fundamental modes in each of the two directions and the high modes.

III. Design of Control Scheme

A. Design of a Command Smoother for Tolerable Vibration

The command smoother is a continuous function, u. The original command is convolved with the smoother, u, to create a smoothed command. The smoothed command can drive the container toward the desired state with minimum slosh. The smoother for slosh suppression is designed by estimating natural sloshing frequencies and damping ratios. The sloshing frequencies can be easily estimated from (15) by measuring the liquid depth and the container size.

The 3-D sloshing dynamic problem induced by planar excitations can be modeled as a series of second-order harmonic oscillators along the two directions from (24) and (25). The harmonic response of a second-order system from the smoother, u, is

$$f(t)=\int_{\tau=0}^{+\infty} u(\tau)\frac{\omega}{\sqrt{1-\zeta^2}}e^{-\zeta\omega(t-\tau)}\sin\left(\omega\sqrt{1-\zeta^2}(t-\tau)\right)d\tau \tag{33}$$

where ω is the natural frequency of the second-order system, and ζ is the damping ratio. The vibration amplitude of the system response (33) is

$$A(t)=\frac{\omega}{\sqrt{1-\zeta^2}}e^{-\zeta\omega t}\sqrt{[W(\omega,\zeta)]^2+[U(\omega,\zeta)]^2} \tag{34}$$

where

$$W(\omega,\zeta)=\int_{\tau=0}^{+\infty} u(\tau)e^{\zeta\omega\tau}\sin\left(\omega\sqrt{1-\zeta^2}\tau\right)d\tau \tag{35}$$

$$U(\omega,\zeta)=\int_{\tau=0}^{+\infty} u(\tau)e^{\zeta\omega\tau}\cos\left(\omega\sqrt{1-\zeta^2}\tau\right)d\tau. \tag{36}$$

If (35) and (36) are limited to zero, the smoother, u, would cause no residual vibrations. However, the practical system often operates with some degree of uncertainty, which can result from poorly known or time-varying parameters and nonlinearities of the system. Accordingly, the smoother, u, could hardly suppress the vibration to zero on an actual system. Thus, the designer hopes that the vibration at the modeled point could be suppressed to a tolerable level [40]

$$\left[e^{-\zeta\omega T_c}\sqrt{[W(\omega,\zeta)]^2+[U(\omega,\zeta)]^2}\right]_{\substack{\omega=\omega_m\\ \zeta=\zeta_m}}=V_{\text{tol}} \tag{37}$$

where V_{tol} is the tolerable level of the vibration, ω_m is the modeled frequency, ζ_m is the modeled damping ratio, and T_c is the duration of the smoother. In addition, the smoother should be robust to the system parameters. The robustness to errors in the natural frequency could be maximized by forcing the vibrations at the modified frequencies, $p\cdot\omega_m$ and $r\cdot\omega_m$, to zero, where p and r are the amending factors. The zero-vibration constraints at the modified frequencies are given by

$$\left[\int_{\tau=0}^{+\infty} u(\tau)e^{\zeta\omega\tau}\sin\left(\omega\sqrt{1-\zeta^2}\tau\right)d\tau\right]_{\substack{\omega=p\omega_m\\ \zeta=\zeta_m}}=0 \tag{38}$$

$$\left[\int_{\tau=0}^{+\infty} u(\tau)e^{\zeta\omega\tau}\cos\left(\omega\sqrt{1-\zeta^2}\tau\right)d\tau\right]_{\substack{\omega=p\omega_m\\ \zeta=\zeta_m}}=0 \tag{39}$$

$$\left[\int_{\tau=0}^{+\infty} u(\tau)e^{\zeta\omega\tau}\sin\left(\omega\sqrt{1-\zeta^2}\tau\right)d\tau\right]_{\substack{\omega=r\omega_m\\ \zeta=\zeta_m}} = 0 \quad (40)$$

$$\left[\int_{\tau=0}^{+\infty} u(\tau)e^{\zeta\omega\tau}\cos\left(\omega\sqrt{1-\zeta^2}\tau\right)d\tau\right]_{\substack{\omega=r\omega_m\\ \zeta=\zeta_m}} = 0. \quad (41)$$

A constraint must be added to increase the robustness of the smoother under variations in the system natural frequency. The derivative of (34) with respect to ω_m should be limited to zero [41]

$$\left[\frac{d\left[\left(e^{-\zeta\omega T_c}W(\omega,\zeta)\right)^2+\left(e^{-\zeta\omega T_c}U(\omega,\zeta)\right)^2\right]}{d\omega}\right]_{\substack{\omega=\omega_m\\ \zeta=\zeta_m}} = 0. \quad (42)$$

Another constraint must be added to ensure the smoother reach the same set-point as the original command. To satisfy the requirement, the integral of the smoother is limited to one [42]

$$\int_{\tau=0}^{+\infty} u(\tau)d\tau = 1. \quad (43)$$

While assuming that p is larger than r, and from (37)–(43), the time-optimal solution of the smoother is described by [43]

$$u(\tau) = \begin{cases} \mu\left(e^{-r\zeta_m\omega_m\tau} - e^{-p\zeta_m\omega_m\tau}\right), 0 \le \tau \le \left(\frac{T_m}{p}\right) \\ \mu e^{-r\zeta_m\omega_m\tau}(1-\delta), \left(\frac{T_m}{p}\right) < \tau < \left(\frac{T_m}{r}\right) \\ \mu\left(\sigma e^{-p\zeta_m\omega_m\tau} - \delta e^{-r\zeta_m\omega_m\tau}\right), \left(\frac{T_m}{r}\right) \\ \quad \le \tau \le (T_m/p + T_m/r) \\ 0, \quad \text{others} \end{cases} \quad (44)$$

where

$$\delta = e^{2\pi\left(\frac{r}{p-1}\right)\frac{\zeta_m}{\sqrt{1-\zeta_m^2}}} \quad (45)$$

$$\sigma = e^{2\pi\left(\frac{p}{r-1}\right)\frac{\zeta_m}{\sqrt{1-\zeta_m^2}}} \quad (46)$$

$$\mu = \frac{pr\zeta_m\omega_m}{(p-r)\left(1-e^{\frac{-2\pi\zeta_m}{\sqrt{1-\zeta_m^2}}}\right)^2} \quad (47)$$

$$T_m = 2\pi/\left(\omega_m\sqrt{1-\zeta_m^2}\right). \quad (48)$$

Convolving the original command with the smoother (44) produces a smoothed command to drive the container inducing a tolerable vibration. In this case, instead of forcing the vibration to zero at the modeling frequency, the vibration is limited to the tolerable level. In addition, forcing the vibrations to zero at the two modified frequencies increases robustness to errors in the natural frequency. The zero derivative constraint ensures that the vibration ranged between the two modified frequencies could be suppressed below the tolerable level. The duration of the smoother (44) is given by

$$T_c = \left(\frac{1}{p}+\frac{1}{r}\right)\cdot T_m. \quad (49)$$

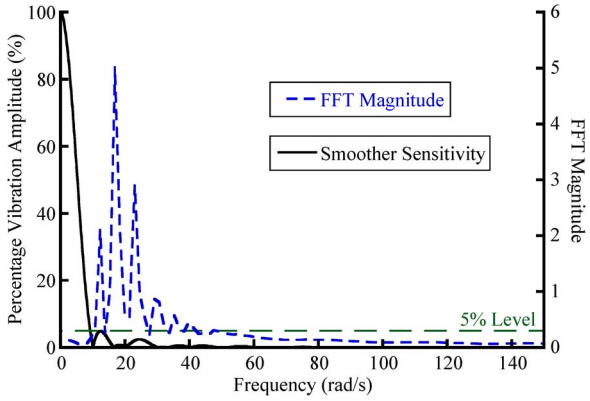

Fig. 4. Frequency sensitivity curve for the smoother and FFT magnitude of a slosh response.

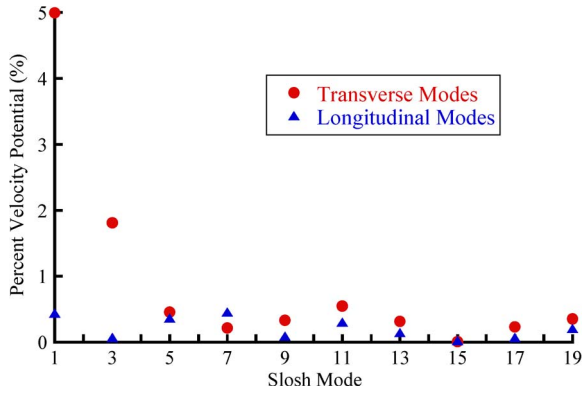

Fig. 5. Percent velocity potential from the smoother.

To better identify the slosh suppression, the fast Fourier transform (FFT) of a slosh response is shown in Fig. 4. The estimates of the sloshing frequencies from the (15) are revealed by the peaks of the FFT magnitude at 12.4, 17.3, 22.5 rad/s, etc. Note that the frequencies of the first transverse mode and longitudinal mode are 12.4 and 17.3 rad/s, respectively. Using the frequency of the first transverse mode (12.4 rad/s, corresponding to the first mode along the long side of the container) as design frequency, the smoother (44) would suppress slosh induced by both the two fundamental modes and high sloshing modes. The amending factors p and r can be calculated by solving the (37) and (42). Numerical solutions in this case are $p = 1.3444$ and $r = 0.8110$ when the tolerable level was set to 5%. While the duration of the smoother is 0.9985 s, the smoother has a rise time (10% to 90%) of 0.5376 s in this case. Fig. 4 also shows the frequency sensitivity curve for the smoother. It is clear that the smoother has a low-pass filtering effect. The 5% insensitivity of the smoother is from 9.3 rad/s to infinity. Thus, the smoother could suppress a wide range of frequencies.

To better evaluate slosh suppression for high modes along the two directions, the ratio of the velocity potential with the smoother to that without the controller is defined as the percent velocity potential [39]. Fig. 5 shows the percent velocity potential resulting from the smoother in each of the two directions. The percentage velocity potential for the first transverse mode is 5%. This is because the vibration at the modeling frequency was

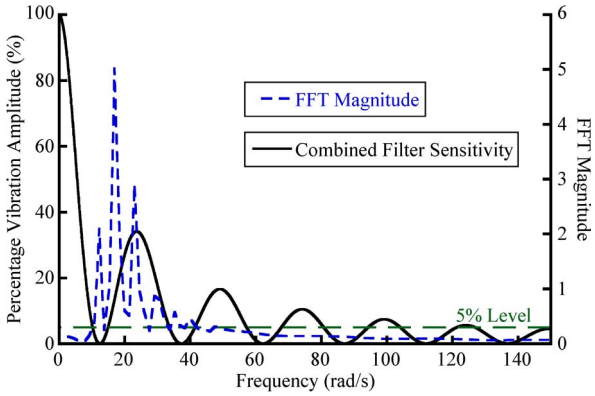

Fig. 6. Frequency sensitivity curve for the combined filter and FFT magnitude of a slosh response.

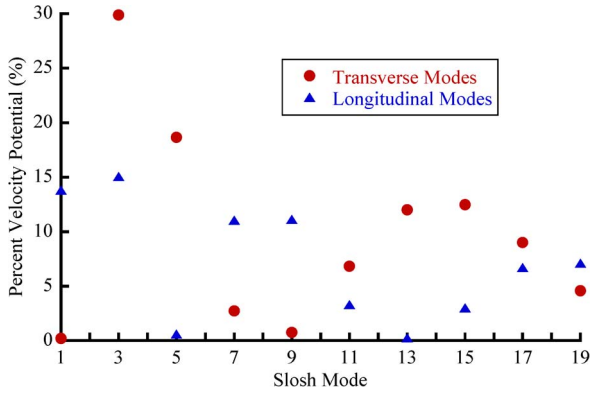

Fig. 7. Percent velocity potential from the combined filter.

limited to the tolerable level. Nonetheless, the smoother can reduce the percent velocity potential for the two fundamental and high modes along the two directions below the 5% level.

B. Combining Input Shaper and Low-Pass Filter

A similar design is the combination of the input shaper and low-pass filter [44]. The combination is achieved by convolving an input shaper with a low-pass filter to suppress vibrations for multimode systems with a few low modes and a range of high modes. The input shaper eliminates the specific low frequencies, and the low-pass filter attenuates higher frequencies. The zero vibration and derivative (ZVD) input shaper is described by [41]

$$\text{ZVD} = \begin{bmatrix} A_i \\ t_i \end{bmatrix} = \begin{bmatrix} \frac{1}{(1+K)^2} & \frac{2K}{(1+K)^2} & \frac{K^2}{(1+K)^2} \\ 0 & \frac{T_m}{2} & T_m \end{bmatrix} \tag{50}$$

where K is given by

$$K = e^{\left(\frac{-\pi\zeta_m}{\sqrt{1-\zeta_m^2}}\right)}. \tag{51}$$

The low-pass filter is given by [30]

$$G_l(s) = \frac{1}{T_l s + 1} \tag{52}$$

where T_l is the time constant of the low-pass filter. The ZVD shaper (50) can be designed by using the frequency and damping ratio of the first transverse mode.

To provide a fair comparison with the smoother (44), the combined filter was designed with the same rise time (10% to 90%) as the smoother. Because the rise time of the smoother is 0.5376 s, the time constant, T_l, of the low-pass filter (52) is found to be 0.1058 s. Note that the duration of the combined filter is infinite.

Fig. 6 shows the frequency sensitivity curve for the combined filter and the FFT magnitude of the slosh response shown in Fig. 4. The combined filter eliminates the specific low frequencies and higher frequencies but cannot limit the slosh below the 5% level for the frequencies between 14.95 and 33.65 rad/s. Note that the 5% insensitivity of the combined filter is much weaker than that of the smoother. In addition, the low-pass filter (52) fails to exploit the known properties of the sloshing dynamics. While the low-pass filtering effect can reduce vibrations, it incurs a large rise-time penalty [44].

Fig. 7 shows the percent velocity potential resulting from the combined filter in each of the two directions. While the percentage velocity potential for the first transverse mode is limited below a very low level, the percentage velocity potential for the first longitudinal mode reaches 13.8%. The percentage velocity potential for some specific modes is eliminated because of the ZVD input shaper. Increasing sloshing modes decreases the percentage velocity potential in both directions because of the low-pass filtering effect. The combined filter cannot reduce the percentage velocity potential below the 5% level for the transverse modal response of the third, the fifth, the 11th, the thirteenth, the fifteenth, and the seventeenth mode. In addition, the percentage velocity potential cannot be suppressed below the 5% level for the longitudinal modal response of the first, the third, the seventh, the ninth, the seventeenth, and the nineteenth mode. This is because the combined filter cannot limit the vibration below the 5% level at these corresponding frequencies.

The presented smoother in this paper is similar to the combined filter previous proposed in [44]. Both are the combination of notch and low-pass filters. The difference is that the smoother can provide more insensitivity to changes in sloshing frequency. However, the design and implementation become more complicated.

C. Robustness Verification of the Methods

This section presents numerical robustness verification of the smoother and the combined filter over a large range of motions and liquid depths. Simulations were conducted using the first ten modes in each of the two directions.

Fig. 8 shows the transient deflection and residual amplitude induced by varying resultant driving distances when the liquid depth and driving angle were fixed at 90 mm and 30°, respectively. The uncontrolled transient deflection increases with an increasing driving distance before 5.8 cm because the amount of transient deflection depends on the size of the acceleration pulse and the duration of the transient stage. After this point, the transient deflection is dependent on the interference between the vibrations caused by the acceleration and deceleration. When the vibration induced by the deceleration is in phase

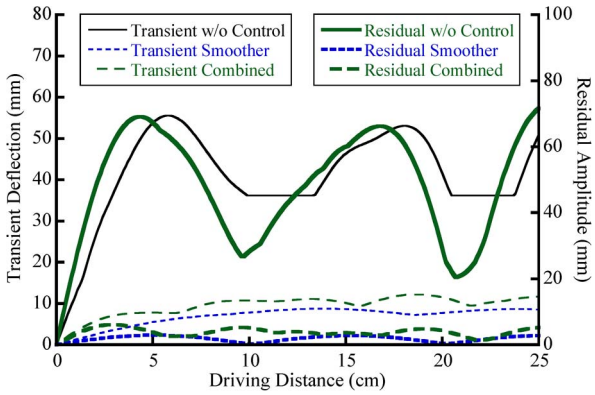

Fig. 8. Transient deflection and residual amplitude against driving distance.

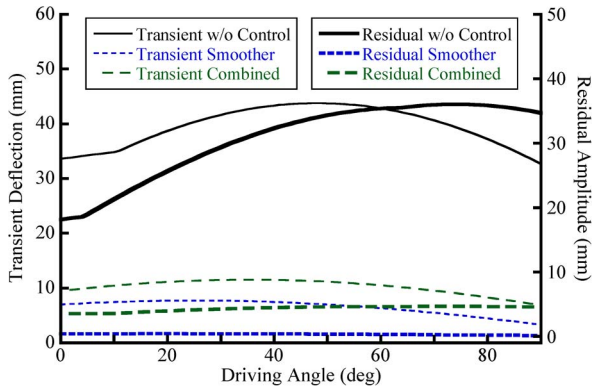

Fig. 9. Transient deflection and residual amplitude against driving angle.

with that caused by the acceleration, the peaks will arise in the uncontrolled transient deflection shown in Fig. 8. When the vibrations caused by the acceleration and deceleration are out of phase, the troughs occur. The uncontrolled residual amplitude demonstrated in Fig. 8 is also the result of the interference between the vibrations caused by the acceleration and deceleration. The smoother and the combined filter attenuated the transient deflection by an average of 83.1% and 76.8%, respectively. The smoother produced a smooth velocity profile to drive the container. The smooth transitions between boundary conditions reduced the transient slosh. In addition, the smoother and the combined filter eliminated the residual amplitude by an average of 96.2% and 92.1%, respectively. This is because the smoother is more insensitive at the frequencies ranged from 14.95 and 33.65 rad/s. The smoother reduces both the transient and residual slosh to a lower level for varying driving motions.

Fig. 9 illustrates the transient deflection and residual amplitude for various driving angles when the resultant driving distance and liquid depth were fixed at 20 cm and 90 mm, respectively. There is only transverse modal response for a zero driving angle. In addition, the container is longitudinally moved for a driving angle of 90°. The total dynamic response is the sum of the transverse modal response and longitudinal modal response. The uncontrolled transient deflection increases as the driving angle increases before 48° and then decreases after that. This is the result of the interference between the transverse modal response and longitudinal modal response.

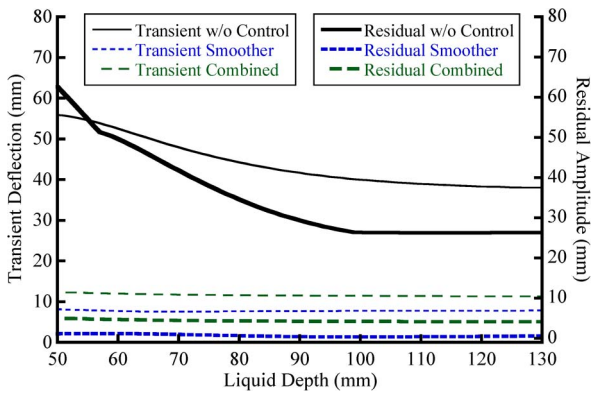

Fig. 10. Transient deflection and residual amplitude against liquid depth.

The uncontrolled residual amplitude increases with increasing driving angle and reaches the maximum value at the driving angle of 75°. The smoother suppressed the transient deflection and residual amplitude by an average of 83.5% and 98.9%, respectively. Meanwhile, the combined filter reduced the transient deflection and residual amplitude by an average of 74.1% and 85.9%, respectively. It demonstrates that the smoother has better performance at reducing the transient and residual slosh caused by the excitation in the random direction.

In many cases, liquid depth may not be known. Then, it becomes important for the controller to have insensitivity to the changes in the liquid depth. The transient deflection and residual amplitude as a function of liquid depth are shown in Fig. 10 when the smoother and the combined filter were designed for a liquid depth of 90 mm. The resultant driving distance and driving angle were fixed at 20 cm and 30°, respectively. Without the controller, large vibrations are induced by the container motion. The uncontrolled transient deflection and residual amplitude decrease with increasing liquid depth, then they slightly change as the liquid depth increases after the container width. The smoother and the combined filter suppressed the transient deflection by an average of 82.4% and 73.6%, respectively. Meanwhile, the smoother and the combined filter reduced the residual amplitude by an average of 98.1% and 87.5%, respectively. The residual amplitudes with the smoother are limited to near-zero values for all the liquid depths shown in Fig. 10. This is because the smoother provides more insensitivity to the changes in the frequency for a wide range of liquid depths.

Figs. 8–10 demonstrated that the proposed method can robustly suppress both the transient and residual slosh for varying working conditions and system parameters.

IV. Experimental Results

Experiments were conducted on a testing apparatus shown in Fig. 11. A liquid container is mounted to an XY gantry that is driven transversely and longitudinally by the Panasonic AC servomotors with encoders. The control hardware consists of a personal computer for program development and user interface, a DSP-based motion control card connecting servo amplifiers to a Visual C++ program. The original command is sent to the program, which applies the smoother or combined filter

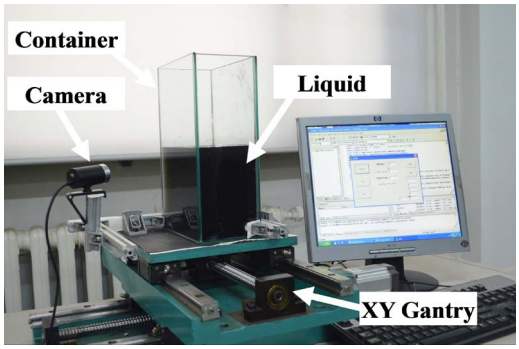

Fig. 11. Experimental testing apparatus.

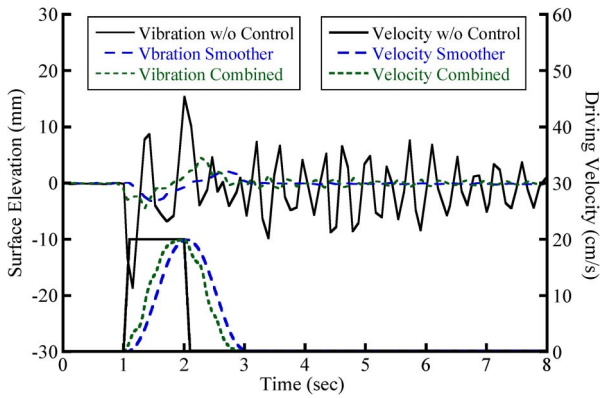

Fig. 12. Experimental slosh response to a driving command.

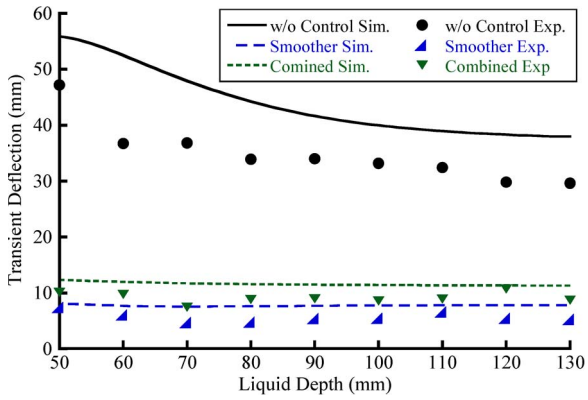

Fig. 13. Experimental transient deflection for various liquid depths.

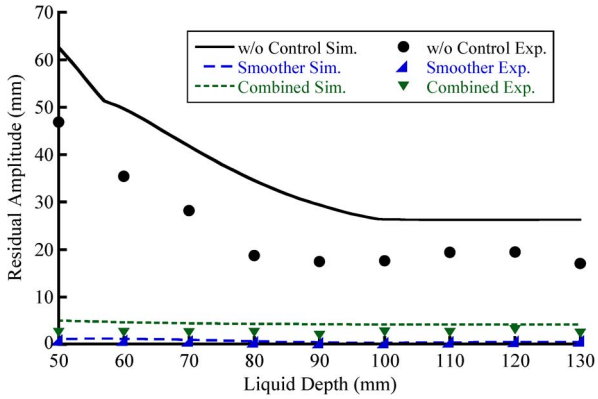

Fig. 14. Experimental residual amplitude for various liquid depths.

algorithm and generates the shaped command for the drives. The size of the container was 182 mm × 102 mm × 200 mm. A CMOS camera was also mounted to the gantry to record surface elevation at the diagonal corner of the container. The liquid depth in the experiment was measured via a plastic ruler.

Fig. 12 shows the experimental response of surface elevation at the diagonal corner of the container caused by the trapezoidal-velocity command. The container was driven when the resultant distance, driving angle, and liquid depth were fixed at 20 cm, 30°, and 90 mm, respectively. The container was still and the surface was level between 0 and 1 s. Then, the container accelerated at 1 s, which induced slosh, and the container decelerated 1.0 s later, which induced additional slosh. The transient deflection and residual amplitude without the controller were 34.0 and 17.4 mm, respectively. The uncontrolled residual amplitude was smaller than the transient deflection because the slosh caused by the deceleration attenuated that induced by the acceleration. Experiment results also show that the transient deflection and residual amplitude with the smoother were 5.4 and 0.4 mm, respectively. In addition, the transient deflection and residual amplitude with the combined filter were 9.0 and 2.6 mm, respectively. It demonstrates that both the smoother and the combined filter can suppress the transient and residual slosh, but the smoother limits the transient and residual slosh to a lower level.

To verify the dynamics and the effectiveness of the smoother on suppressing slosh for variations of system parameters and working conditions, one set of experiments were performed. According to the simulations shown in Section III, variations in the liquid depth were selected to test a wide range of possible dynamics in the following experiments. The container was driven at a distance of 20 cm with the driving angle fixed at 30°. The liquid depth ranged from 50 to 130 mm, whereas the smoother and the combined filter were designed for a liquid depth of 90 mm. Fig. 13 shows the simulated and experimental results of the transient slosh from those tests. Without the controller, the transient slosh slowly decreased with increasing liquid depth. The experimental results were better than the simulated value because liquid was assumed to be inviscid and the surface tension was ignored. Experimental results show that the smoother and the combined filter suppressed the transient slosh by an average of 83.7% and 73.8%, respectively. Thus, the smoother has better performance to reduce the transient slosh. This is because the smooth velocity profile produced by the smoother benefits reduction of the transient slosh.

Fig. 14 shows the simulated and experimental residual amplitudes for various liquid depths. Increasing liquid depth decreased the uncontrolled residual amplitude. The experimental results were better than the simulated value for this case. It is also because liquid was assumed to be inviscid and the surface tension was ignored. The smoother reduced the residual slosh to < 0.92 mm for all depths tested, and the combined filter limited the residual slosh to < 3.1 mm for all cases. Experimental results show that the smoother limited the residual slosh to a lower level because the smoother is more insensitive to the changes in the sloshing frequency.

Those experiments verified that the smoother can effectively suppress the 3-D slosh for a wide range of various system parameters as it was predicted by the simulations in Figs. 8–10.

V. Conclusion

This paper has presented theoretical and experimental analyses of the dynamic effects and control of the 3-D slosh in a moving rectangular liquid tank. The slosh suppression is challenging because the dynamics is very complicated. A command smoothing technique was proposed to reduce both the two fundamental modes and an infinite number of sloshing modes. A comparison between the presented method and the previously proposed combined filter has been conducted. Both the smoother and combined filter produced a robust control effect for various system parameters and working conditions. However, the smoother can provide more robustness to changes in the frequency. Therefore, it limited the transient and residual slosh to a lower level. Simulated and experimental results were used to verify key dynamic behavior and the effectiveness of the method.

References

[1] W. Rumold, "Modeling and simulation of vehicles carrying liquid cargo," *Multibody Syst. Dyn.*, vol. 5, no. 4, pp. 351–374, May 2001.

[2] C. Nichkawde, P. Harish, and N. Ananthkrishnan, "Stability analysis of a multibody system model for coupled slosh-vehicle dynamics," *J. Sound Vib.*, vol. 275, no. 3–5, pp. 1069–1083, Aug. 2004.

[3] M. Grundelius and B. Bernhardsson, "Control of liquid slosh in an industrial packaging machine," in *Proc. IEEE Int. Conf. Control Appl.*, Kohala Coast, HI, USA, 1999, pp. 1654–1659.

[4] T. Acarman and Ü. Özgüner, "Rollover prevention for heavy trucks using frequency shaped sliding mode control," *Veh. Syst. Dyn.*, vol. 44, no. 10, pp. 737–762, Oct. 2006.

[5] K. Muto, Y. Kasai, and M. Nakahara, "Experimental tests for suppression effects of water restraint plates on sloshing of a water pool," *J. Pressure Vessel Technol.*, vol. 110, no. 3, pp. 240–246, Aug. 1988.

[6] V. Modi and S. Munshi, "An efficient liquid sloshing damper for vibration control," *J. Fluids Struct.*, vol. 12, no. 8, pp. 1055–1071, Nov. 1998.

[7] T. Ikeda and R. Ibrahim, "Passive vibration control of structures subjected to random ground excitation utilizing sloshing in rectangular tanks," *J. Pressure Vessel Technol.*, vol. 136, no. 1, pp. 011801-1–011801-11, Oct. 2013.

[8] R. Venugopal and D. Bernstein, "State space modeling and active control of slosh," in *Proc. IEEE Int. Conf. Control Appl.*, Dearborn, MI, USA, 1996, pp. 1072–1077.

[9] H. Sira-Ramirez and M. Fliess, "A flatness based generalized PI control approach to liquid sloshing regulation in a moving container," in *Proc. Amer. Control Conf.*, Anchorage, AK, USA, 2002, pp. 2909–2914.

[10] B. Bandyopadhyay, P. Gandhi, and S. Kurode, "Sliding mode observer based sliding mode controller for slosh-free motion through PID scheme," *IEEE Trans. Ind. Electron.*, vol. 56, no. 9, pp. 3432–3442, Sep. 2009.

[11] S. Kurode, S. Spurgeon, B. Bandyopadhyay, and P. Gandhi, "Sliding mode control for slosh-free motion using a nonlinear sliding surface," *IEEE/ASME Trans. Mechatronics*, vol. 18, no. 2, pp. 714–724, Apr. 2013.

[12] H. Richter, "Motion control of a container with slosh: Constrained sliding mode approach," *J. Dyn. Syst., Meas., Control*, vol. 132, no. 3, pp. 031002-1–031002-10, Apr. 2010.

[13] T. Acarman and U. Ozguner, "Rollover prevention for heavy trucks using frequency shaped sliding mode control," in *Proc. IEEE Int. Conf. Control Appl.*, Istanbul, Turkey, 2003, pp. 7–12.

[14] K. Yano and K. Terashima, "Robust liquid container transfer control for complete sloshing suppression," *IEEE Trans. Control Syst. Technol.*, vol. 9, no. 3, pp. 483–493, May 2001.

[15] K. Terashima and G. Schmidt, "Motion control of a cart-based container considering suppression of liquid oscillations," in *Proc. IEEE Int. Symp. Ind. Electron.*, Santiago, Chile, 1994, pp. 275–280.

[16] M. Reyhanoglu and J. Hervas, "Nonlinear modeling and control of slosh in liquid container transfer via a PPR robot," *Commun. Nonlinear Sci. Numer. Simul.*, vol. 18, no. 6, pp. 1481–1490, Jun. 2013.

[17] M. Reyhanoglu and J. Hervas, "Nonlinear dynamics and control of space vehicles with multiple fuel slosh modes," *Control Eng. Pract.*, vol. 20, no. 9, pp. 912–918, Sep. 2012.

[18] M. Reyhanoglu and J. Hervas, "Robotically controlled sloshing suppression in point-to-point liquid container transfer," *J. Vib. Control*, vol. 19, no. 14, pp. 2137–2144, Oct. 2013.

[19] J. Feddema *et al.*, "Control for slosh-free motion of an open container," *IEEE Control Syst. Mag.*, vol. 17, no. 1, pp. 29–36, Feb. 1997.

[20] S. Chen, B. Hein, and H. Worn, "Using acceleration compensation to reduce liquid surface oscillation during a high speed transfer," in *Proc. IEEE Int. Conf. Robot. Autom.*, Roma, Italy, 2007, pp. 2951–2956.

[21] K. Terashima, M. Hamaguchi, and K. Yano, "Modeling and input shaping control of liquid vibration for an automatic pouring system," in *Proc. 35th IEEE Conf. Decis. Control*, Kobe, Japan, 1996, pp. 4844–4850.

[22] B. Pridgen, K. Bai, and W. Singhose, "Shaping container motion for multimode and robust slosh suppression," *J. Spacecraft Rockets*, vol. 50, no. 2, pp. 440–448, Feb. 2013.

[23] K. Terashima and K. Yano, "Sloshing analysis and suppression control of tilting-type automatic pouring machine," *Control Eng. Pract.*, vol. 9, no. 6, pp. 607–620, Jun. 2001.

[24] A. Aboel-Hassan, M. Arafa, and A. Nassef, "Design and optimization of input shapers for liquid slosh suppression," *J. Sound Vib.*, vol. 320, no. 1/2, pp. 1–15, Feb. 2009.

[25] H. Abramson, *The Dynamic Behavior of Liquids in Moving Containers*, vol. 106. Washington, DC, USA: NASA, 1966.

[26] F. Dodge, "The new dynamic behavior of liquids in moving containers," Southwest Res. Inst., San Antonio, TX, USA, Tech. Rep. SP-106, 2000, Chap. 2.

[27] R. Ibrahim, V. Pilipchuk, and T. Ikeda, "Recent advances in liquid sloshing dynamics," *Appl. Mech. Rev.*, vol. 54, no. 2, pp. 133–199, Mar. 2001.

[28] P. Gandhi, K. Joshi, and N. Ananthkrishnan, "Design and development of a novel 2DOF actuation slosh rig," *J. Dyn. Syst., Meas., Control*, vol. 131, no. 1, p. 011006, Dec. 2008.

[29] P. Gandhi, J. Mohan, K. Joshi, and N. Ananthkrishnan, "Development of 2DOF actuation slosh rig: A novel mechatronic system," in *Proc. IEEE Int. Conf. Ind. Technol.*, Bombay, India, 2006, pp. 1810–1815.

[30] K. Yano and K. Terashima, "Sloshing suppression control of liquid transfer systems considering a 3-D transfer path," *IEEE/ASME Trans. Mechatronics*, vol. 10, no. 1, pp. 8–16, Feb. 2005.

[31] K. Yano, T. Toda, and K. Terashima, "Sloshing suppression control of automatic pouring robot by hybrid shape approach," in *Proc. 40th IEEE Conf. Decis. Control*, Orlando, FL, USA, 2001, pp. 1328–1333.

[32] J. Xu, Z. Guo, and T. H. Lee, "Design and implementation of integral sliding-mode control on an underactuated two-wheeled mobile robot," *IEEE Trans. Ind. Electron.*, vol. 61, no. 7, pp. 3671–3681, Jul. 2014.

[33] X. Zhang, Y. Fang, and N. Sun, "Minimum-time trajectory planning for underactuated overhead crane systems with state and control constraints," *IEEE Trans. Ind. Electron.*, vol. 61, no. 12, pp. 6915–6925, Dec. 2014.

[34] W. He, S. Zhan, and S. Ge, "Adaptive control of a flexible crane system with the boundary output constraint," *IEEE Trans. Ind. Electron.*, vol. 61, no. 8, pp. 4126–4133, Aug. 2014.

[35] R. Ibrahim, *Liquid Sloshing Dynamics: Theory and Applications*. London, U.K.: Cambridge Univ. Press, 2005.

[36] G. Bao and Z. Wang, "Finite element method for eigen problem of liquid 3D sloshing," *Chin. Quart. Mech.*, vol. 24, no. 2, pp. 185–190, Jun. 2003.

[37] G. Bao, "Equivalent mechanical model of liquid sloshing horizontal cylindrical container," *J. Shanghai Jiaotong Univ.*, vol. 37, no. 12, pp. 1961–1968, Dec. 2003.

[38] C. Oh, B. Sun, Y. Park, and W.-R. Roh, "Sloshing analysis using ground experimental apparatus," in *Proc. Int. Conf. Control, Autom. Syst.*, Seoul, Korean, 2008, pp. 2203–2207.

[39] Q. Zang, J. Huang, and Z. Liang, "Slosh suppression for infinite modes in a moving liquid container," *IEEE/ASME Trans. Mechatronics*, vol. 20, no. 1, pp. 217–225, Feb. 2015.

[40] W. Singhose, W. Seering, and N. Singer, "Residual vibration reduction using vector diagrams to generate shaped inputs," *J. Mech. Des.*, vol. 116, no. 2, pp. 654–659, Jun. 1994.

[41] N. Singer and W. Seering, "Preshaping command inputs to reduce system vibration," *J. Dyn. Syst., Meas., Control*, vol. 112, no. 1, pp. 76–82, Mar. 1990.

[42] X. Xie, J. Huang, and Z. Liang, "Vibration reduction for flexible systems by command smoothing," *Mech. Syst. Signal Process.*, vol. 39, no. 1/2, pp. 461–470, Aug. 2013.

[43] X. Xie, J. Huang, and Z. Liang, "Using continuous function to generate shaped command for vibration reduction," *Proc. Inst. Mech. Eng. J. Syst. Control Eng.*, vol. 227, no. 6, pp. 523–528, Jun. 2013.
[44] W. Singhose, R. Eloundou, and J. Lawrence, "Command generation for flexible systems by input shaping and command smoothing," *J. Guid., Control Dyn.*, vol. 33, no. 6, pp. 1697–1707, Dec. 2010.

Qiang Zang received the Bachelor's degree from Hunan University, Changsha, China, in 2012. He is currently working toward the master's degree in mechanical engineering at Beijing Institute of Technology, Beijing, China.

His research interests include the area of sloshing dynamics and control.

Jie Huang received the Ph.D. degree in mechanical engineering from Beijing Institute of Technology, Beijing, China, in 2004.

He then joined the Faculty of the School of Mechanical Engineering, Beijing Institute of Technology. He held a visiting appointment with Georgia Institute of Technology, Atlanta, GA, USA. His research interests include dynamics and control of mechanical systems.